Archival Report

Biological Psychiatry

Fragile X Syndrome Patient–Derived Neurons Developing in the Mouse Brain Show *FMR1*-Dependent Phenotypes

Marine A. Krzisch, Hao Wu, Bingbing Yuan, Troy W. Whitfield, X. Shawn Liu, Dongdong Fu, Carrie M. Garrett-Engele, Andrew S. Khalil, Tenzin Lungjangwa, Jennifer Shih, Aaron N. Chang, Stephen Warren, Angela Cacace, Kristin R. Andrykovich, Rosalie G.J. Rietjens, Owen Wallace, Mriganka Sur, Bhav Jain, and Rudolf Jaenisch

ABSTRACT

BACKGROUND: Fragile X syndrome (FXS) is characterized by physical abnormalities, anxiety, intellectual disability, hyperactivity, autistic behaviors, and seizures. Abnormal neuronal development in FXS is poorly understood. Data on patients with FXS remain scarce, and FXS animal models have failed to yield successful therapies. In vitro models do not fully recapitulate the morphology and function of human neurons.

METHODS: To mimic human neuron development in vivo, we coinjected neural precursor cells derived from FXS patient–derived induced pluripotent stem cells and neural precursor cells derived from corrected isogenic control induced pluripotent stem cells into the brain of neonatal immune-deprived mice.

RESULTS: The transplanted cells populated the brain and a proportion differentiated into neurons and glial cells. Immunofluorescence and single and bulk RNA sequencing analyses showed accelerated maturation of FXS neurons after an initial delay. Additionally, we found increased percentages of Arc- and Egr-1–positive FXS neurons and wider dendritic protrusions of mature FXS striatal medium spiny neurons.

CONCLUSIONS: This transplantation approach provides new insights into the alterations of neuronal development in FXS by facilitating physiological development of cells in a 3-dimensional context.

https://doi.org/10.1016/j.biopsych.2022.08.020

In fragile X syndrome (FXS), the expansion of the CGG triplet repeats in the *FMR1* gene leads to hypermethylation of the repeats and of the *FMR1* promoter. This causes the transcriptional silencing of the *FMR1* gene and the reduction or absence of the *FMR1* protein, FMRP (1). FMRP is an RNA-binding protein and is thought to be a translational repressor at the synapse, whose absence causes defects in neuronal development (2).

Data on FXS patients remain scarce, and findings from animal models of FXS have failed to translate into successful therapies, highlighting the need for human cell–based models. In vitro studies using human stem cell–derived neurons (3–10) have yielded discrepant results. Canonical 2-dimensional culture conditions fail to fully recapitulate the morphological and functional characteristics of human neurons. Additionally, impaired cell type specification due to ectopic activation of stress pathways was found in cerebral organoids, the most commonly used 3-dimensional in vitro model. Transplantation of the organoids in the mouse cortex alleviated these limitations (11). Thus, transplantation of human neural progenitor cells (hNPCs) into the mouse brain may better reflect physiological cellular behavior than in vitro models. hNPCs transplanted into the neonatal mouse brain migrate away from the injection site, differentiate into neurons, mature, express brain region–specific markers, and become electrically active (12–14).

Here, we cotransplanted hNPCs, differentiated from FXS patient–derived induced pluripotent stem cells (iPSCs) and from isogenic control iPSCs, in the brain of immune-deprived mouse neonates to study developmental defects of FXS neurons in an in vivo context.

METHODS AND MATERIALS

Experimental Animals

The animals used were NOD/scid/gamma mice. Detailed information is provided in Supplemental Methods.

hNPC Differentiation, Labeling, and Transplantation

Detailed information about hNPC differentiation and labeling is provided in Supplemental Methods. Cultured hNPCs were fully dissociated using Accutase (StemCell Technologies) and resuspended in phosphate-buffered saline without calcium and magnesium prior to injection at a concentration of 10^5 cells/μL. Postnatal day 0 (P0) to P3 mouse pups of either sex

were manually injected with 4×10^5 hNPC in the lateral ventricles (1 anterior and 1 posterior injection site per brain hemisphere) using glass micropipettes.

Transplanted Human Cell Extraction for Single-Cell RNA Sequencing

Mice were euthanized using cervical dislocation. Brains were extracted and dissociated using Miltenyi Adult mouse and rat Brain Dissociation Kit (130-107-677; Miltenyi Biotec) and the gentleMACS Octo Dissociator. The cells were resuspended in phosphate-buffered saline + 0.5% bovine serum albumin and stained with DAPI to determine viability. DAPI-GFP$^+$ and DAPI-mCherry$^+$ cells were isolated using fluorescence-activated cell sorting (FACS) and immediately sent for single-cell or bulk RNA sequencing (RNA-seq).

Single-Cell RNA-Seq Analysis

Sequencing data were mapped to a reference metagenome composed of human (GRCh38), mouse (GRCm38), GFP, and mCherry sequences with Cell Ranger (v.3.1.0). We analyzed the high-quality human cells with Seurat v.3 (15). To determine cell types in the different clusters, we used marker genes, cell cycle markers, and a comparison with a published single-cell RNA-seq dataset from the human embryonic primary cortex (16). Differential gene analysis between FXS and control was performed using edgeR (17) on pseudo-bulk RNA-seq counts. Genes with locally adjusted p value $< .05$ and at least 2-fold effect sizes were considered to be differentially expressed. We performed gene list enrichment analysis on the differentially expressed protein-coding genes using ToppFun from the ToppGene suite (18,19). Detailed information is provided in Supplemental Methods.

Bulk RNA-Seq and Analysis

Only the reads uniquely mapped to human reference were assigned to genes. Gene expression levels were normalized by library size. Differential expression analysis based on negative binomial distribution was done with DESeq2 (20). Detailed information is provided in Supplemental Methods.

NanoString Profiling

Samples were run on a NanoString SPRINT according to manufacturer's instructions. The results were analyzed using the nSolver Analysis Software. Detailed information is in Supplemental Methods.

DNA Methylation Analysis

Pyro-sequencing of bisulfite-converted genomic DNA samples was performed with the PyroMark Q48 Autoprep (Qiagen) according to the manufacturer's instructions. Primer information is listed in Table 1.

Table 1. Primer Information for Pyro-sequencing of Bisulfite-Converted Genomic DNA Samples

Primer Name	Primer Sequence
hFmr1_For	GAATTGGGATAATAGGATGTATTTGATTTT
hFmr1_Rev_Bio	CCCTCTCTCTTCAAATAACCT
hFmr1_Seq	TTTAGTTTTTTAGTTTTTTATTAAG

Reverse Transcriptase–Quantitative Polymerase Chain Reaction

RNA was extracted using miRNeasy Micro Kit (Qiagen) and converted to complementary DNA (cDNA) using qScript cDNA Super Mix (Quanta Biosciences). rt-qPCR were prepared with Fast SYBR Green Master Mix (Life Technologies), and performed using a QuantStudio 6 machine. Primer information is listed in Table 2.

Immunohistochemistry and Immunocytochemistry

Immunostainings were performed using antibodies listed in Tables S2 and S3. Detailed information is provided in Supplemental Methods.

Neuronal Imaging, Tracing, and Morphometric Analyses

Arborization Analysis. Confocal microscopy z-stacks of control and FXS neurons were acquired with a 20× dry objective (zoom 0.6), converted to grayscale images with Fiji software (22), and traced using Neuromantic freeware (Darren Myat, https://www.reading.ac.uk/neuromantic/body_index.php) in semiautomatic mode.

Dendritic Spine Width and Density Analysis. Confocal microscopy z-stacks of control and FXS proximal dendritic segments were acquired with a 40× oil objective (zoom 4). The z-stepsize was 0.456 µm (wavelength 488 nm) or 0.497 µm (wavelength 594 nm). Images were deconvolved using Huygens and a theoretical point-spread function, and 3-dimensional automated analysis of dendritic protrusion density and width was performed using the Filament Tracer function of the Imaris software (RRID:SCR_007370) as previously described (23). The maximum spine length and minimum spine end diameter were set at 5 and 0.215 µm, respectively.

Statistical Analyses of Immunofluorescence Experiments. Statistical analyses were performed using GraphPad Prism (v.8) (RRID:SCR_002798). Detailed information is provided in Supplemental Methods.

RESULTS

Differentiation and Migration of Transplanted hNPCs

To investigate the developmental phenotypes of FXS neurons in vivo, we used 2 different FXS or corrected isogenic control pairs (Table S1). In the FXS_SW/C1_2_SW pair, the isogenic

Table 2. Primer Information for RT-qPCR

Primer Name	Primer Sequence
hFmr1_For (21)	GTATGGTACCATTTGTTTTTGTG
hFmr1_Rev (21)	CATCATCAGTCACATAGCTTTTTTC
human beta-Actin_qPCR_For (8)	CATGTACGTTGCTATCCAGGC
human beta-Actin_qPCR_Rev (8)	CTCCTTAATGTCACGCACGAT

RT-qPCR, reverse transcriptase–quantitative polymerase chain reaction.

control C1_2_SW was generated by CRISPR (clustered regularly interspaced short palindromic repeats)-mediated deletion of the CGG repeats in the FXS patient–derived male FXS_SW iPSC line (24), leading to the reactivation of the *FMR1* promoter and FMRP re-expression. In the FX2 dCT/FX2 dCdT pair, the FXS patient–derived male FXS2 iPSC line was targeted with a catalytically inactive Cas9 fused to Tet1 as previously described (8,25). This led to the demethylation of the CGG repeats, reactivation of the *FMR1* promoter, and FMRP re-expression (FX2 dCT iPSC line). To generate a control where the CGG repeats were not demethylated, the FXS2 iPSC line was targeted with a catalytically inactive Cas9 fused to a catalytically inactive Tet1 (FX2 dCdT iPSC line) (Figure S4). To eliminate potential off-target effects associated with methylation editing, we compared the FX2 dCT iPSC line and its isogenic control FX2 dCdT iPSC line in all the experiments.

hNPCs were generated from mutant and control iPSCs and labeled with GFP (control) or mCherry (FXS) (Figure 1A). It was found that 85% ± 4% C1_2_SW GFP hNPCs, 86% ± 0.4% FXS_SW mCherry hNPCs, 94% ± 0.04% dCas9-Tet1, and 90% ± 7% dCas9-dTet1 hNPCs coexpressed Pax6, Sox2 and Nestin, 3 hNPC markers, showing high purity of cultured hNPCs. In addition, 4% ± 8% dCas9-dTet1 hNPCs were only positive for Sox2 and Nestin (Figure S5A). The *FMR1* promoter was efficiently demethylated in control hNPCs, and they expressed *FMR1* as assessed by reverse

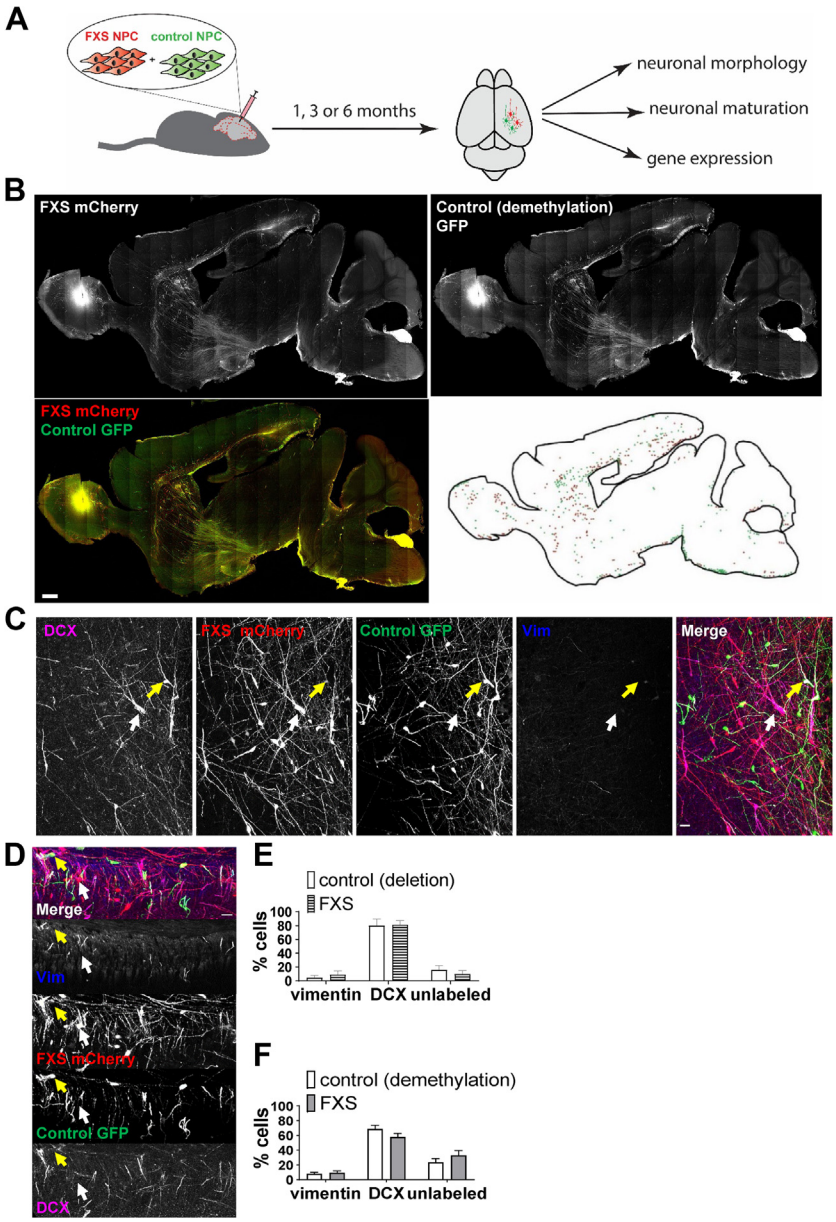

Figure 1. Transplanted hNPCs populate several areas of the brain and differentiate into neurons and astrocytes. **(A)** Coinjection of FXS hNPCs labeled with mCherry and isogenic control hNPCs labeled with GFP in the cerebral ventricles of NSG mouse neonates. Brains were harvested at 1, 3, or 6 months PI. **(B)** Maximum intensity projection of a 100-µm-thick mouse brain slice at 1 month PI. Scale bar = 200 µm. Red: mCherry-labeled FXS; green: GFP-labeled isogenic control (demethylation). Right lower panel: localization of the cell bodies of transplanted FXS (red) and isogenic control (green) cells. **(C)** Transplanted hNPCs from FXS and isogenic control (demethylation) labeled with DCX at 1 month PI. **(D)** Transplanted FXS and isogenic control (demethylation) hNPCs labeled with vim at 1 month PI. Red: mCherry-labeled FXS; green: GFP-labeled isogenic control. The yellow and the white arrow show the cell body of a control and FXS cell, respectively. Scale bars = 50 µm. **(E)** Percentage of FXS and isogenic control (deletion) cells labeled with vim, DCX, or unlabeled at 1 month PI. Two-way repeated-measures ANOVA; N = 4 animals, 17–109 neurons per animal for each group. **(F)** Percentage of FXS and isogenic control (demethylation) cells labeled with vim, DCX, or unlabeled at 1 month PI. Two-way repeated-measures ANOVA; N = 4 animals, 118–140 neurons per animal for each group. Bar heights and whiskers represent the mean ± SEM. ANOVA, analysis of variance; DCX, doublecortin; FXS, fragile X syndrome; GFP, green fluorescent protein; hNPC, human neural progenitor cell; PI, post injection; vim, vimentin.

transcriptase–quantitative polymerase chain reaction (rt-qPCR). In contrast, *FMR1* promoter methylation was preserved in FXS hNPCs, and they did not express *FMR1* (Figure S5B–D). Henceforth, the FXS_SW/C1_2_SW and dCas9-Tet1/dCas9-dTet1 pairs will be referred to as deletion pair: control (deletion)/FXS and demethylation pair: control (demethylation)/FXS, respectively.

We coinjected hNPCs derived from FXS and control cell lines into the brain ventricles of immune-deficient mouse neonates (Figure 1A) and analyzed the brains at different time points post injection (PI). Transplanted hNPCs migrated through the mouse brain and populated several areas, including the hippocampus, cortex, striatum, thalamus, and midbrain at 1 month PI (Figure 1B). The rostral migratory stream (RMS) is the migratory route of neurons generated in the subventricular zone to the olfactory bulb. At 15 days PI, a high proportion of cells was present in the corpus callosum (CC), and some cells were present in the RMS (Figure S6A). At 1 month PI, no cells were present in the RMS, and fewer cells were present in the CC (Figure 1B). This suggests that transplanted hNPCs integrated the CC before migrating to other brain areas and used the RMS to migrate to the olfactory bulb, although the design of our study did not allow us to determine their exact path of migration. This migration pattern has also been described in human-mouse microglial chimeras (26), suggesting that the migration of human cells injected in the ventricles is guided by mechanical rather than chemical factors.

Although the localization of transplanted cells varied from injection to injection, no obvious difference in migration or selective survival inside a brain area was detected between FXS and control at 15 days and 1 month PI (Figure S7). Transplanted cells occasionally formed aggregates along the spinal cord but did not integrate (data not shown). Transplanted cells also formed aggregates in the mouse brain (Figure S6), mainly composed of neurons, glial cells, and hNPCs (data not shown). All the transplanted cells were human nuclei antigen-positive, confirming their human origin (Figure S8).

We analyzed transplanted control and FXS cells present in the hippocampus, striatum, cortex, midbrain, and thalamus and pooled them together for quantification. We matched FXS neurons with control neurons localized in the same brain areas. Most of the hNPCs had differentiated into doublecortin (DCX)-positive immature neurons at 1 month PI with a small proportion of hNPCs (~10%) positive for vimentin, a marker of glial cells and hNPCs (Figure 1C–F). A small proportion of cells were positive for Olig2, a marker for all cells of the oligodendrocyte lineage (27,28), in the deletion pair (Figure S9): 7% ± 3% control and 0.9% ± 0.9% FXS (4 animals, 101–138 cells per animal). No transplanted cell was $Olig2^+$ at 1 month PI in the demethylation pair (4 animals, 100 cells per animal). Importantly, oligodendrocyte progenitors can also express DCX (29), although at lower levels than immature neurons. We found no $Olig2^+/DCX^+$ transplanted cell at 1 month PI (Figure S9). Additionally, no $vimentin^+/DCX^+$ cell was found (Figure 1C–E). This indicates that our antibody against DCX can reliably detect immature neurons at 1 month PI. FXS and control hNPCs yielded similar fractions of immature neurons at 1 month PI (Figure 1C–E).

After 1 month PI, the axonal projection density of transplanted cells decreased, indicating a decrease in neuron survival (Figure S6B, C), and glial proliferation occurred. Most $NeuN^+$ neurons located in the brain regions studied were stained with markers specific to the brain region, such as Cux1, Ctip2, Brn2 (cortex), FoxP1 (striatum), MATH2 (hippocampus), Otx2 (midbrain), and Gbx2 (thalamus), at 3 months PI. The proportion of positive neurons was similar in control and FXS neurons for each marker (Figure S10). Importantly, of 20 neurons analyzed per marker per cell line outside of the area where mouse neurons were positive for a given marker, none were positive, indicating that the staining of transplanted neurons was specific to the brain region. This suggests that most transplanted neurons differentiated into the proper neuronal subtype in the brain areas studied.

Approximately 60% to 80% of control transplanted neurons were FMRP positive at 1, 3, and 6 months PI, and none of the FXS cells were FMRP positive at the same time points (Figure S11A–C), showing that transplanted control neurons retained stable FMRP expression in vivo. Moreover, the demethylation of the *FMR1* promoter was maintained, and rt-qPCR showed robust expression of the *FMR1* gene in control (deletion pair) transplanted cells at 1 month PI (Figure S11D–F).

Altered Maturation Process of Transplanted FXS Neurons

DAPI is predominantly impermeable to live cells and can be used as a cell viability dye, DAPI-negative cells being considered viable. To investigate gene expression phenotypes of transplanted FXS neurons, we collected GFP^+DAPI^- and $mCherry^+DAPI^-$ control and FXS viable transplanted neurons from the deletion pair by whole-brain extraction and subsequent FACS sorting. We performed single-cell RNA sequencing on the cells using the 10x Genomics platform. We analyzed 2 engrafted mouse brains at 1 month PI. GFP^+ cells and $mCherry^+$ cells represented 0.8% ± 0.11% and 0.1% ± 0.01% of the total $DAPI^-$ cells, respectively.

FXS and control cells were assigned to similar UMAP clusters, allowing comparison of FXS and control cells within the same clusters (Figure S12A). Control and FXS cells were composed of neural precursor cells (NPCs), neurons at different maturation stages, and glial cells (detailed information is provided in Supplemental Methods) and showed similar developmental trajectories (Figure S12B, C).

Gene list enrichment analysis of the differentially expressed genes between FXS and control neuronal clusters (immature neurons 1 and 2; more mature neurons 1 and 2) indicated the upregulation of neurogenesis, neuronal differentiation, and synaptic signaling (Figure 2A). During neuronal differentiation, NPCs exit the cell cycle and differentiate into neuroblasts. Cell division pathways were downregulated in FXS neurons (Figure 2B). We analyzed the numbers of FXS and control cells in each cluster and found that the proportion of NPCs in FXS cells decreased, whereas the proportion of immature and mature neurons increased (Figure S13). The apoptosis pathway was not significantly upregulated in FXS NPCs and neurons in the gene set enrichment analysis (30) (Figure S13B,

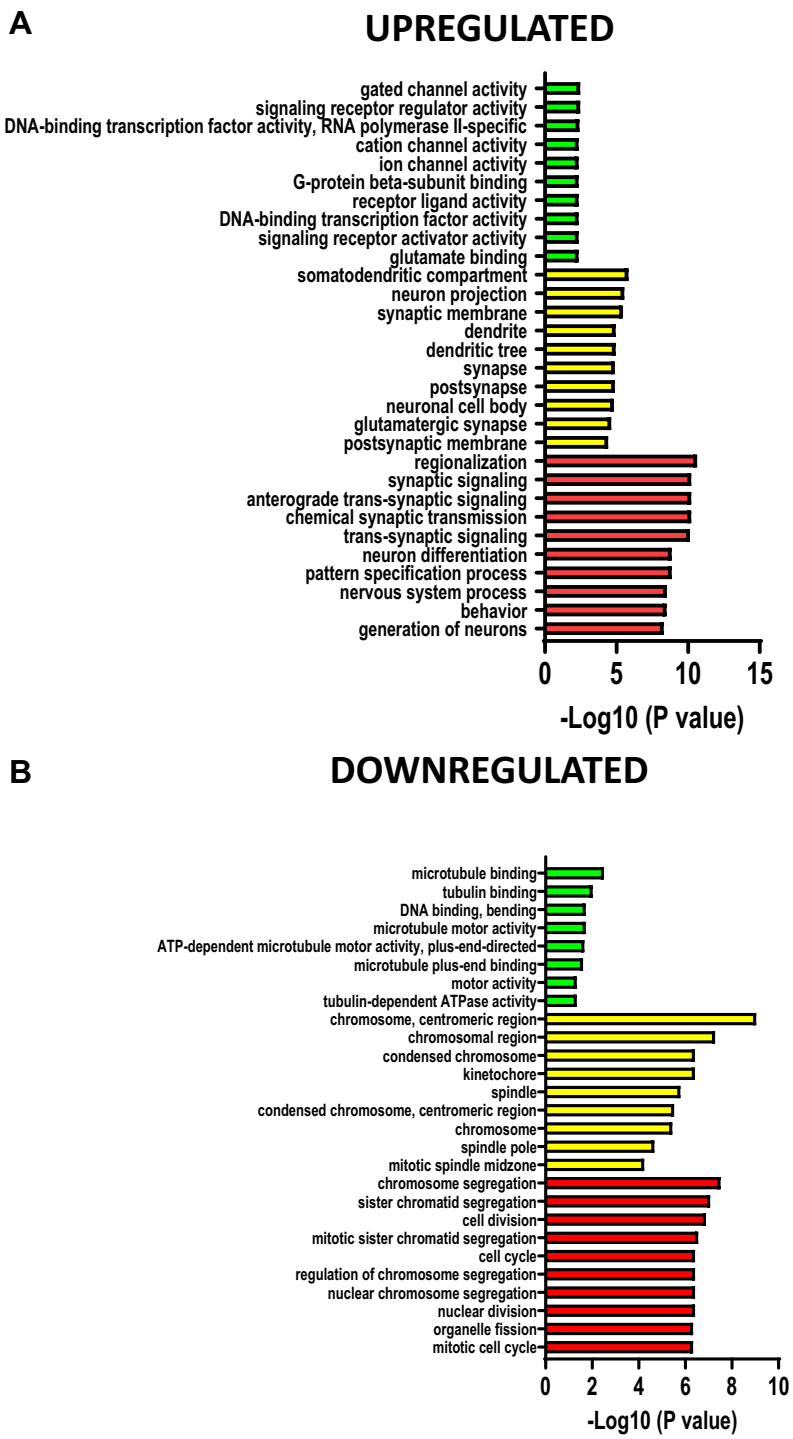

Figure 2. Gene list enrichment analysis reveals upregulation of neuronal differentiation, synaptic signaling, and neuronal development pathways and downregulation of cell division pathways in FXS neurons from the deletion pair. Ten most significantly upregulated **(A)** and downregulated **(B)** gene pathways in FXS neurons from the deletion pair were assessed by single-cell RNA sequencing (green: molecular function; yellow: cell component; red: biological process). n = 2 animals. FXS, fragile X syndrome.

C). Additionally, the percentage of mitochondrial genes was similar between FXS and control cells (Figure S13D). Together, these results suggest that cell death was similar in control and FXS cells after extraction and sorting, and there was increased maturation of FXS cells in the deletion pair at 1 month PI.

FMR1 was significantly downregulated in FXS neurons compared with control ($\log_2$ fold change = −4, p = 1.44 ×

10^{-32}); however, only 7% of control cells showed *FMR1* expression (Figure S14). This is likely due to the low sequencing depth of the 10x Genomics platform and/or the low level of *FMR1* expression in the cells, as 60% of FXS neurons were FMRP positive as assessed by immunofluorescence.

The upregulated genes in FXS neurons included a known target of FMRP, *NKX2-2* (31) (Figure S15 and Table S4). *NKX2-2* upregulation was significant in neurons but not in NPCs. *NKX2-2* expression was undetectable in the glial cell cluster (Figure S15B). NKX2-2 upregulation was confirmed by NanoString analysis at 1 month PI (Figure S15C). This is consistent with the role of FMRP as a translational repressor.

To further investigate alterations in the maturation of FXS neurons, we analyzed transplanted neurons on brain slices using immunofluorescence. Neuroblasts initially express doublecortin (DCX), an immature neuron marker, then gradually lose DCX expression and start expressing NeuN, a mature neuron marker (32). The proportion of DCX^+ neurons decreased, and the proportion of $NeuN^+$ neurons increased between 15 days PI and 3 months PI (Figure 3A–G), showing ongoing neuronal maturation. At 6 months PI, no DCX^+ cell was found, suggesting that transplanted neurons had undergone full maturation.

We analyzed transplanted control and FXS cells present in the hippocampus, striatum, cortex, midbrain, and thalamus and pooled them together for quantification. We matched FXS neurons with $FMRP^+$ control neurons localized in the same brain areas. The maturation stage of FXS and $FMRP^+$ control neurons was assessed by evaluating the fraction of DCX^+,

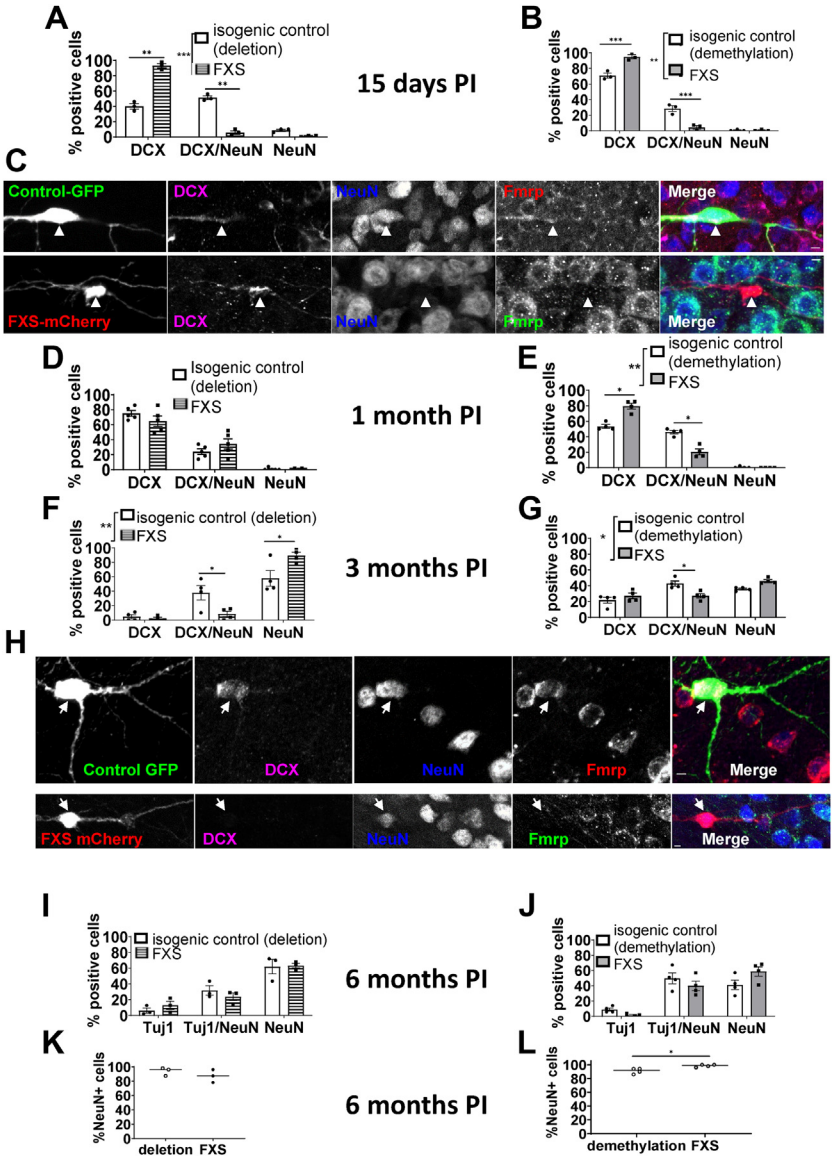

Figure 3. Altered maturation process of transplanted FXS neurons compared with isogenic control. Percentage of DCX, doublecortin$^+$ NeuN$^+$ (DCX/NeuN) and NeuN$^+$ (NeuN) cells at 15 days PI in control and FXS cells from the deletion pair **(A)** and from the demethylation pair **(B)**. Repeated-measures two-way ANOVA followed by Šídák's multiple comparisons test; n = 3 animals, 51–55 neurons per mouse per group. **(C)** Confocal maximum intensity projection of isogenic control (deletion) (upper panel) and FXS (lower panel) neurons immunostained with DCX and NeuN at 15 days PI. White arrows indicate the cell bodies of neurons. The FXS neuron is stained with DCX only, whereas the control neuron shows DCX/NeuN costaining, indicating a more advanced stage of maturation of the control neuron. Scale bars = 5 μm. Percentage of doublecortin$^+$ (DCX), doublecortin$^+$ NeuN$^+$ (DCX/NeuN) and NeuN$^+$ (NeuN) cells at 1 month PI in control and FXS cells from the deletion pair **(D)** and from the demethylation pair **(E)**. Repeated-measures two-way ANOVA followed by Šídák's multiple comparisons test; n = 4 animals, 30–72 neurons per mouse per group. Percentage of DCX, doublecortin$^+$ NeuN$^+$ (DCX/NeuN), and NeuN$^+$ (NeuN) cells at 3 months PI in control and FXS cells from the deletion pair **(F)** and from the demethylation pair **(G)**. Repeated-measures two-way ANOVA followed by Šídák's multiple comparisons test; n = 4 animals, 45–73 neurons per mouse per group. **(H)** Confocal maximum intensity projection of isogenic control (demethylation) (upper panel) and FXS (lower panel) neurons immunostained with DCX and NeuN at 3 months PI. The FXS neuron is stained with NeuN only, whereas the control neuron shows DCX/NeuN costaining, indicating a more advanced stage of maturation of the FXS neuron. White arrows indicate the cell bodies of neurons. Scale bars = 5 μm. Percentage of Tuj1$^+$, Tuj1$^+$ NeuN$^+$ (Tuj1/NeuN), and NeuN$^+$ (NeuN) cells at 6 months PI in control and FXS cells from the deletion pair **(I)** and from the demethylation pair **(J)**. Repeated-measures two-way ANOVA; n = 3–4 animals, 49–55 neurons per mouse per group. Total percentage of NeuN$^+$ cells at 6 months PI in control and FXS cells from the deletion pair **(K)** and from the demethylation pair **(L)**. Paired t test; n = 3–4 animals, 49–55 neurons per mouse per group. *$p < .05$. Bar heights and whiskers represent the mean ± SEM. ANOVA, analysis of variance; DCX, doublecortin; FXS, fragile X syndrome; PI, post injection.

$DCX^+/NeuN^+$, and $NeuN^+$ cells in the total of cells staining for DCX and/or NeuN at 15 days, 1 month, and 3 months PI. As no DCX^+ transplanted neuron was found at 6 months PI, the maturation stage at 6 months PI was assessed using Tuj1, a generic neuronal marker expressed from midneuronal maturation that keeps being expressed in a subpopulation of mature neurons, and NeuN. We determined the percentage of $Tuj1^+$, $Tuj1^{+/-}NeuN^+$, and $NeuN^+$ neurons cells in the total of cells staining for Tuj1 and/or NeuN.

At 15 days PI, the percentage of DCX^+ neurons and the percentage of DCX^+NeuN^+ neurons were, respectively, increased and decreased in FXS cells, indicating that the maturation of FXS neurons was initially delayed (Figure 3A–C). The effect of the *FMR1* mutation was similar in all the brain regions studied at this time point (Figure S16). At 1 month PI, the fraction of neurons labeled with DCX and/or NeuN was similar between FXS and deletion control, suggesting that there was no difference in maturation between control and FXS neurons for this pair (Figure 3D). In contrast, fewer FXS neurons were labeled with NeuN in the demethylation pair, indicating that FXS neurons were more immature than control neurons at that stage (Figure 3E). We used bulk RNA sequencing to confirm the decreased maturity of FXS neurons in extracted cells from the demethylation pair at 1 month PI (Figure S17). GFP^+ cells and $mCherry^+$ cells represented 1.8% ± 0.69% and 0.05% ± 0.0.02% of the total $DAPI^-$ cells, respectively. Pathways linked to neuronal development were downregulated, confirming that at 1 month PI, FXS cells were less mature than control in the demethylation pair (Figure S17B). *NKX2-2* was also upregulated in this pair (Table S4), and upregulation was confirmed by NanoString analysis at 1 month PI (Figure S15C). *FMR1* was the only gene downregulated in both pairs.

At 3 months PI, however, for both isogenic pairs, the proportion of $NeuN^+$ neurons was increased, indicating increased maturation of FXS neurons at this later stage (Figure 3F–H). At 6 months PI, virtually all $Tuj1^+$ cells expressed NeuN, suggesting that FXS and control neurons had reached full maturation at this time point. A small but significant increase in the percentage of $NeuN^+$ FXS cells compared with control was still present for the demethylation pair, in line with accelerated maturation of FXS neurons (Figure 3I–L).

Together, these observations suggest that the maturation of transplanted FXS neurons is, after an initial delay, accelerated compared with control. The differences between the 2 pairs at 1 and 6 months PI may stem from the fact the FXS cell line from the demethylation pair (FXS2) displayed slower neuronal maturation compared with the FXS cell line from the deletion pair (FXS_SW), as indicated by increased percentages of DCX^+ neurons and decreased percentages of $NeuN^+$ neurons in FXS2 compared with FXS_SW at all time points studied. As a result, the initial delay in maturation persisted at 1 month in FXS2 neurons but not in FXS_SW neurons, and accelerated maturation compared with control was still visible at 6 months in FXS2 but not in FXS_SW neurons.

Increased Immediate Early Gene Expression and Dendritic Spine Size in Transplanted FXS Neurons

Previous work by our group and others showed that FXS neurons in both isogenic pairs are hyperexcitable in vitro (8,9). Immediate early genes (IEGs) are expressed during synaptic plasticity and are commonly used as markers for synaptic activity. To determine whether IEGs were upregulated in FXS neurons, we used immunofluorescence to assess *ARC*, *EGR1*, and *FOS* expression in transplanted control and FXS neurons. Neurons were defined by DCX positivity at 1 month PI, as most neurons express DCX at this time point and by NeuN staining at 3 and 6 months PI because most neurons express this marker at these later time points. At 1 month PI, a higher fraction of FXS neurons from the deletion pair was Arc^+ compared with control (Figure 4A). No significant difference was observed in the demethylation pair, although the percentage of FXS Arc^+ neurons was slightly higher than in control (Figure 4B). At 3 and 6 months PI, an increased percentage of FXS neurons was Arc^+ compared with control (Figure 4A–C). Similar to Arc labeling, a higher percentage of FXS neurons was Egr-1–positive at all the time points studied (Figure 4D–F). The effect of the *FMR1* mutation on Arc and Egr-1 positivity was similar in all the brain regions studied (Figures S18 and S19). The IEG *FOS* is expressed at lower levels in the mouse brain than *ARC* and *EGR1* (33–36), resulting in a low proportion of c-fos–positive cells in the brain without stimulation. Of 38 to 51 transplanted neurons analyzed, no c-fos–positive control or FXS cells were found at the time points studied. NanoString analysis confirmed increased expression of *ARC* in FXS neurons at 1 month PI. A significant increase in *EGR1* expression was only present in the demethylation pair at 1 month PI (Figure S20). Together, these results suggest increased synaptic activity in FXS neurons.

Next, we assessed the dendritic protrusion density and morphology of mature FXS and control neurons in the striatum at 6 to 7 months PI. Because the striatum was the brain region with the most transplanted human neurons still present at 6 months PI, and as mature medium spiny neurons display complex morphology and high dendritic spine density, we focused our analysis on the medium spiny neurons of the striatum. We used DARPP32 as a marker for mature medium spiny neurons (MSNs) (Figure S21A). No difference in neuronal arborization complexity was detected between FXS and control MSNs (Figure S21B–F). Dendritic spines generally correspond to excitatory synapses (37,38). It is commonly accepted that increased spine head size correlates with increased synaptic strength, and dendritic spines become wider after long-term potentiation (39). We measured dendritic protrusion density and head diameter in control and FXS neurons, using automated tracing and analysis with the Imaris software. Dendritic protrusion end diameter was significantly increased in FXS MSNs in both pairs (Figure 5A–D). We classified dendritic protrusions into 3 categories depending on the size of their head: head size $\leq$ 0.3 μm, 0.3 μm < head size < 0.6 μm, and head size $\geq$ 0.6 μm. For both pairs, FXS neurons had more large protrusions (head size $\geq$ 0.6 μm) and less thin protrusions (0.3 μm < head size < 0.6 μm) than control neurons (Figure 5A, B, E, F). No significant change in dendritic protrusion density was detected (Figure 5G, H). This suggests that although excitatory synaptogenesis in FXS MSNs was unchanged, excitatory synaptic strength was increased. Together, these results suggest increased synaptic activity, but not

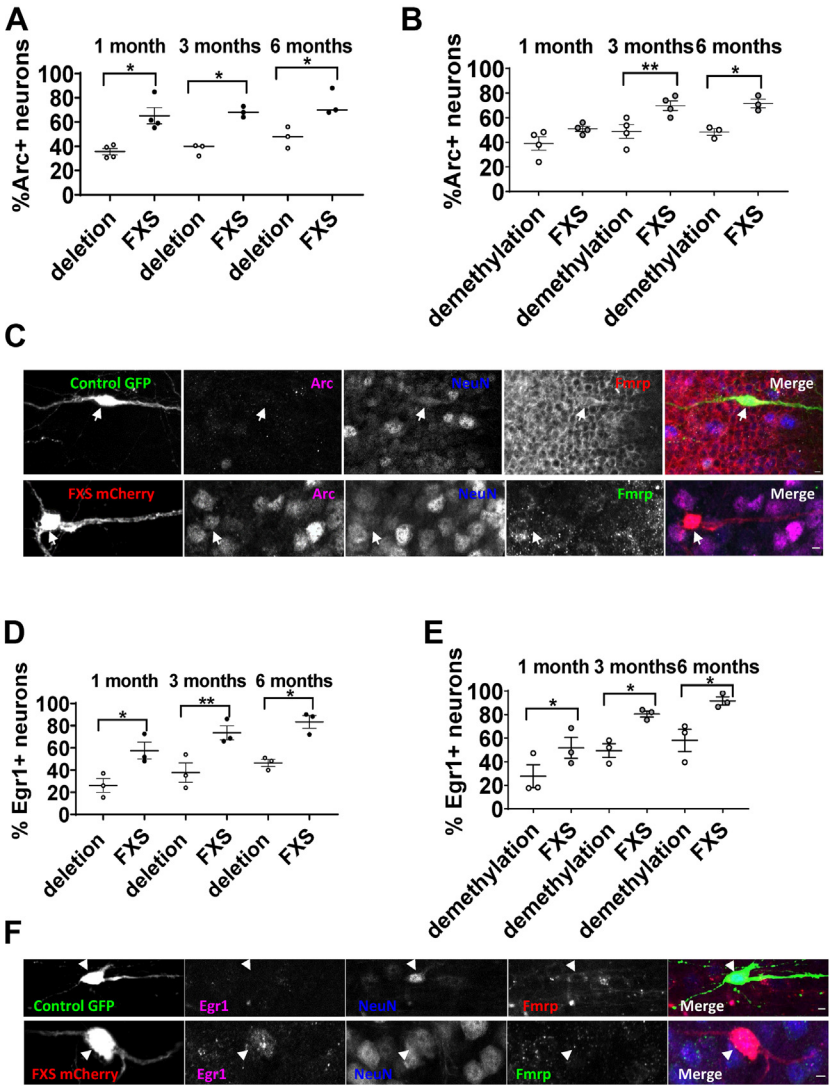

Figure 4. Increased percentages of Arc- and Egr-1–positive transplanted FXS neurons. Percentage of isogenic control and FXS Arc-positive neurons at 1, 3, and 6 months PI in the deletion pair **(A)** and the demethylation pair **(B)**. Paired *t* tests; $n = 3$–4 animals, 36–78 neurons analyzed per group. **(C)** Confocal maximum intensity projections showing an isogenic control (demethylation) Fmrp-positive Arc-negative neuron and an FXS Fmrp-negative Arc-positive neuron at 3 months PI. White arrows indicate neuronal cell bodies. Scale bars = 5 μm. Percentage of isogenic control and FXS Egr-1–positive neurons at 1 month PI, 3 months PI, and 6 months PI for the deletion pair **(D)** and the demethylation pair **(E)**. Paired *t* tests; $n = 3$ animals, 50–56 neurons analyzed per group. **(F)** Confocal maximum intensity projections showing an isogenic control (demethylation) Fmrp-positive Egr-1–negative neuron and an FXS Fmrp-negative Egr-1–positive neuron at 3 months PI. White arrows indicate neuronal cell bodies. Scale bars = 5 μm. Neurons were defined as doublecortin-positive cells at 1 month PI and as NeuN-positive cells at 3 months and 6 months PI. $^{*}p < .05$; $^{**}p < .01$. Data are presented as mean ± SEM. FXS, fragile X syndrome; PI, post injection.

excitatory synaptogenesis, in FXS neurons compared with control.

DISCUSSION

In vitro models do not entirely recapitulate the morphological and physiological properties of neurons. In this study, we cotransplanted FXS and isogenic control hNPCs in the mouse brain, allowing for neuronal development in the in vivo context of the mouse brain. FXS neurons transplanted in the mouse brain showed accelerated maturation after an initial delay, and our data suggest that their synapses are hyperactive.

While we cannot totally exclude interactions between FXS and control cells, integration of transplanted cells was sparse: extraction of transplanted cells yielded an average number of cells of 1.2×10^5 cells per mouse brain, with numbers ranging from 5×10^3 to 2×10^6 cells. This represents only 0.2% of the mouse brain (40), indicating that transplanted cells were mainly surrounded by wild-type mouse cells. Furthermore, various levels of contribution by the transplanted cells yielded the same results.

FXS MSNs displayed an increased dendritic protrusion head diameter. This is not consistent with previous studies showing dendritic protrusion elongation and no change in dendritic protrusion head diameter in mature striatal MSNs in an FXS mouse model (41). Similarly, dendritic spine analysis in patients with FXS showed increased spine density and an increase in the proportion of spines with a longer neck and smaller head in neocortical pyramidal cells (42). This difference may be explained by a noncell autonomous effect on the dendritic spine phenotype, possibly caused by FXS astrocytes. The transplanted FXS and control neurons in our study were exposed to the same neurodevelopmental niche and although FXS glial cells were present in the mouse brain

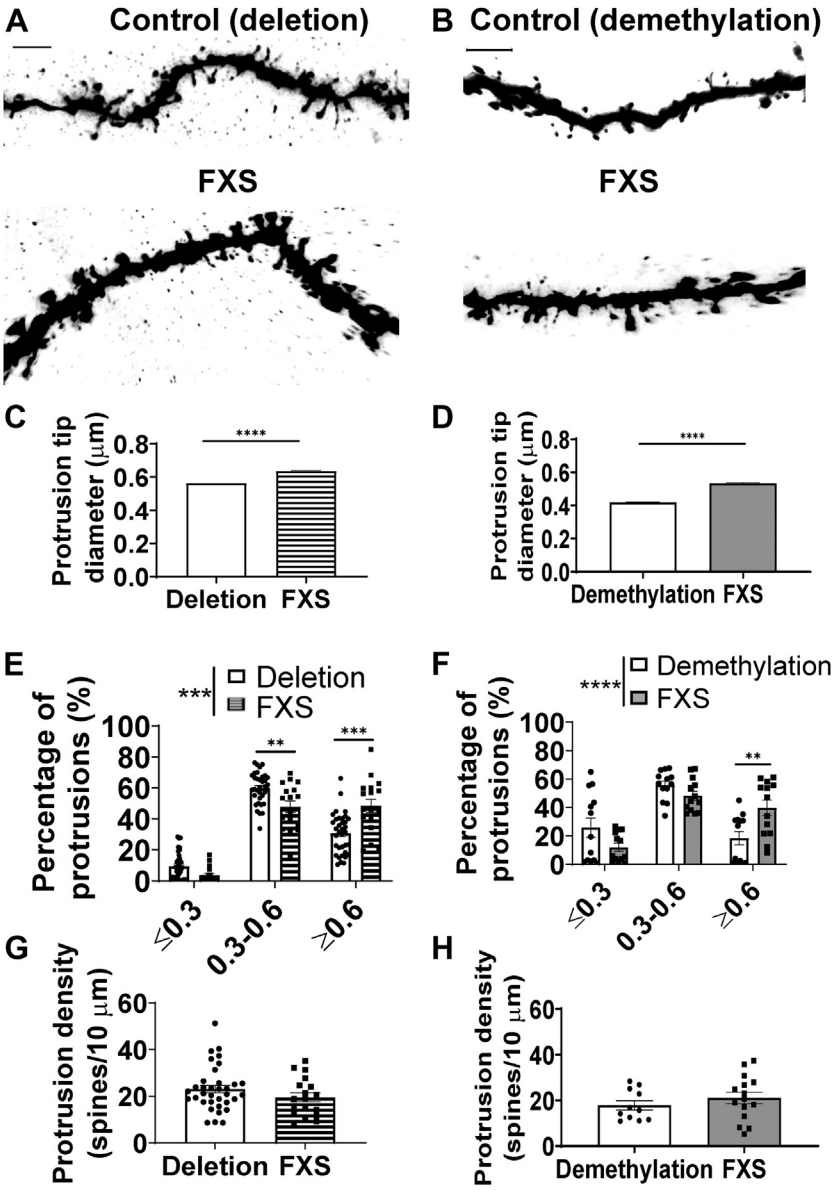

Figure 5. Wider dendritic protrusions in transplanted FXS striatal MSNs at 6–7 months post injection. Representative 3D reconstructions of dendritic segments of control (upper panel) and FXS (lower panel) MSNs in the deletion **(A)** and demethylation **(B)** pairs. Average tip diameter of dendritic protrusions of control and FXS MSNs from the deletion **(C)** and demethylation **(D)** pairs. Unpaired Mann-Whitney test; n = 1945 to 4509 protrusions from 13 to 35 MSNs per group. Percentage of protrusions with tip diameter inferior or equal to 0.3 µm (≤0.3), strictly comprised between 0.3 and 0.6 µm (0.3–0.6), or superior or equal to 0.6 µm (≥0.6) in control and FXS MSNs from the deletion **(E)** and demethylation **(F)** pairs. Mixed-effects model followed by Šídák's correction for multiple comparisons; n = 13–35 MSNs per group. Average protrusion density of FXS and control MSNs from the deletion **(G)** and demethylation **(H)** pairs. n = 11–35 MSNs per group. *$p < .05$; **$p < .01$; ***$p < .001$; ****$p < .0001$. Bar heights and whiskers represent the mean ± SEM. Scale bars = 50 µm. FXS, fragile X syndrome; MSN, medium spiny neuron.

and proliferated between 1 and 6 months PI, they were sparse, and the neurons analyzed were not in direct contact with them. Therefore, the effects we observed were most likely cell autonomous. Consistent with this hypothesis, adult astrocyte-specific *FMR1* knockout mice displayed increased spine density and a higher proportion of thin dendritic spines in the motor cortex, indicating that FXS astrocytes are necessary and sufficient for the dendritic spine phenotype of neurons in FXS (43).

For future work, our transplantation approach could be refined: the number of transplanted neurons decreased between 1 month and 6 months PI, and transplanted neurons were sparse at 6 months PI. Moreover, glial cells proliferated over time, making the analysis at later time points challenging. The fate of the transplanted cells is not controlled in our approach, making the study of different neuronal subtypes difficult. To solve this issue, one could consider injecting cortical or striatal neurons as done in previous studies (44–46). This approach may however give lower contribution of the cells to the mouse brain at early time points because neurons are less resistant to stress than neural progenitor cells and do not proliferate after injection.

ACKNOWLEDGMENTS AND DISCLOSURES

This work was funded by Fulcrum Therapeutics and National Institutes of Health (Grant No. 5R01MH104610-21 [to RJ]).

MK, HW, AC, and RJ conceived the idea for this study. MK and HW designed the experiments. MK interpreted the data. BY and TWW analyzed the single-cell sequencing data. MK, HW, DF, CN, and JS performed the

experiments. MK, CMG, KRA, RR, BJ, and JS analyzed the data. SL provided FXS2 and isogenic control iPSCs. SW provided the FXS_SW and isogenic control iPSCs. OW oversaw the first part of the study. MK and RJ wrote the manuscript with input from all the other authors.

We thank Patti Wisniewski, Patrick Autissier, and Hanna Aharonov from the FACS facility of Whitehead Institute for Biomedical Research for FACS and Jennifer Love from the Genomics core of Whitehead Institute for single-cell sequencing service. We thank George Bell for helpful discussions about statistics. We thank Wendy Salmon from the Keck Microscopy Facility of Whitehead Institute for her useful suggestions on confocal microscopy acquisitions. We thank Steve Warren in Emory University for providing FXS_SW iPSCs lines. We thank members of the Jaenisch lab and Fulcrum Therapeutics for discussion and suggestions on the manuscript. We thank Li-Huei Tsai and her group for providing the dissociator used for the extraction of transplanted cells and Matheus Victor for helping with calcium imaging experiments.

These data were presented during the International Society for Stem Cell Research Annual Meeting 2020–virtual meeting.

A previous version of this article was published as a preprint on bioRxiv: https://doi.org/10.1101/2021.09.27.461739.

RJ is a cofounder of Fate, Fulcrum, and Omega Therapeutics and an adviser to Camp4 and Dewpoint Therapeutics. HW, ANC, AC, and OW were full-time employees of Fulcrum Therapeutics at the time of the study. All other authors report no biomedical financial interests or potential conflicts of interest.

ARTICLE INFORMATION

From the Whitehead Institute for Biomedical Research, Cambridge, Massachusetts (MAK, BY, TWW, DF, CMGE, ASK, TL, KRA, RGJR, BJ, RJ); Full Circles Therapeutics, Inc., Cambridge, Massachusetts (HW); Department of Physiology and Cellular Biophysics, Columbia University Medical Center, New York, New York (XSL); Picower Institute for Learning and Memory, Cambridge, Massachusetts (JS, MS); Prime Medicine, Inc., Cambridge, Massachusetts (ANC); Departments of Human Genetics, Biochemistry, and Pediatrics, Emory University School of Medicine, Atlanta, Georgia (SW); Arvinas, New Haven, Connecticut (AC); Monte Rosa Therapeutics, Boston, Massachusetts (OW); and the Department of Biology, Massachusetts Institute of Technology, Cambridge, Massachusetts (RJ).

Address correspondence to Rudolf Jaenisch, Ph.D., at jaenisch@wi.mit.edu, or Marine A. Krzisch, Ph.D., at mkrzisch@wi.mit.edu.

Received Sep 30, 2021; revised and accepted Aug 11, 2022.

Supplementary material cited in this article is available online at https://doi.org/10.1016/j.biopsych.2022.08.020.

REFERENCES

1. Dahlhaus R (2018): Of men and mice: Modeling the fragile X syndrome. Front Mol Neurosci 11:41.
2. Hagerman RJ, Berry-Kravis E, Hazlett HC, Bailey DB Jr, Moine H, Kooy RF, *et al.* (2017): Fragile X syndrome. Nat Rev Dis Primers 3: 17065.
3. Telias M, Segal M, Ben-Yosef D (2013): Neural differentiation of fragile X human embryonic stem cells reveals abnormal patterns of development despite successful neurogenesis. Dev Biol 374:32–45.
4. Doers ME, Musser MT, Nichol R, Berndt ER, Baker M, Gomez TM, *et al.* (2014): iPSC-derived forebrain neurons from FXS individuals show defects in initial neurite outgrowth. Stem Cells Dev 23:1777–1787.
5. Halevy T, Czech C, Benvenisty N (2015): Molecular mechanisms regulating the defects in fragile X syndrome neurons derived from human pluripotent stem cells. Stem Cell Reports 4:37–46.
6. Sheridan SD, Theriault KM, Reis SA, Zhou F, Madison JM, Daheron L, *et al.* (2011): Epigenetic characterization of the FMR1 gene and aberrant neurodevelopment in human induced pluripotent stem cell models of fragile X syndrome. PLoS One 6:e26203.
7. Utami KH, Skotte NH, Colaço AR, Yusof NABM, Sim B, Yeo XY, *et al.* (2020): Integrative analysis identifies key molecular signatures underlying neurodevelopmental deficits in fragile X syndrome. Biol Psychiatry 88:500–511.
8. Liu XS, Wu H, Krzisch M, Wu X, Graef J, Muffat J, *et al.* (2018): Rescue of fragile X syndrome neurons by DNA methylation editing of the FMR1 gene. Cell 172:979–992.e6.
9. Graef JD, Wu H, Ng C, Sun C, Villegas V, Qadir D, *et al.* (2020): Partial FMRP expression is sufficient to normalize neuronal hyperactivity in fragile X neurons. Eur J Neurosci 51:2143–2157.
10. Brighi C, Salaris F, Soloperto A, Cordella F, Ghirga S, de Turris V, *et al.* (2021): Novel fragile X syndrome 2D and 3D brain models based on human isogenic FMRP-KO iPSCs. Cell Death Dis 12:498.
11. Bhaduri A, Andrews MG, Mancia Leon W, Jung D, Shin D, Allen D, *et al.* (2020): Cell stress in cortical organoids impairs molecular subtype specification. Nature 578:142–148.
12. Chen C, Kim WY, Jiang P (2016): Humanized neuronal chimeric mouse brain generated by neonatally engrafted human iPSC-derived primitive neural progenitor cells. JCI Insight 1:e88632.
13. Reubinoff BE, Itsykson P, Turetsky T, Pera MF, Reinhartz E, Itzik A, *et al.* (2001): Neural progenitors from human embryonic stem cells. Nat Biotechnol 19:1134–1140.
14. Zhou FW, Fortin JM, Chen HX, Martinez-Diaz H, Chang LJ, Reynolds BA, Roper SN (2015): Functional integration of human neural precursor cells in mouse cortex. PLoS One 10:e0120281.
15. Stuart T, Butler A, Hoffman P, Hafemeister C, Papalexi E, Mauck WM 3rd, *et al.* (2019): Comprehensive integration of single-cell data. Cell 177:1888–1902.e21.
16. Polioudakis D, de la Torre-Ubieta L, Langerman J, Elkins AG, Shi X, Stein JL, *et al.* (2019): A single-cell transcriptomic atlas of human neocortical development during mid-gestation. Neuron 103:785–801.e8.
17. McCarthy DJ, Chen Y, Smyth GK (2012): Differential expression analysis of multifactor RNA-Seq experiments with respect to biological variation. Nucleic Acids Res 40:4288–4297.
18. Chen J, Xu H, Aronow BJ, Jegga AG (2007): Improved human disease candidate gene prioritization using mouse phenotype. BMC Bioinformatics 8:392.
19. Kaimal V, Bardes EE, Tabar SC, Jegga AG, Aronow BJ (2010): ToppCluster: A multiple gene list feature analyzer for comparative enrichment clustering and network-based dissection of biological systems. Nucleic Acids Res 38:W96–102.
20. Love MI, Huber W, Anders S (2014): Moderated estimation of fold change and dispersion for RNA-seq data with DESeq2. Genome Biol 15:550.
21. Park CY, Halevy T, Lee DR, Sung JJ, Lee JS, Yanuka O, *et al.* (2015): Reversion of FMR1 methylation and silencing by editing the triplet repeats in fragile X iPSC-derived neurons. Cell Rep 13:234–241.
22. Schindelin J, Arganda-Carreras I, Frise E, Kaynig V, Longair M, Pietzsch T, *et al.* (2012): Fiji: An open-source platform for biological-image analysis. Nat Methods 9:676–682.
23. Swanger SA, Yao X, Gross C, Bassell GJ (2011): Automated 4D analysis of dendritic spine morphology: Applications to stimulus-induced spine remodeling and pharmacological rescue in a disease model. Mol Brain 4:38.
24. Xie N, Gong H, Suhl JA, Chopra P, Wang T, Warren ST (2016): Reactivation of FMR1 by CRISPR/Cas9-mediated deletion of the expanded CGG-repeat of the fragile X chromosome. PLoS One 11: e0165499.
25. Liu XS, Wu H, Ji X, Stelzer Y, Wu X, Czauderna S, *et al.* (2016): Editing DNA methylation in the mammalian genome. Cell 167:233–247.e17.
26. Xu R, Li X, Boreland AJ, Posyton A, Kwan K, Hart RP, *et al.* (2020): Human iPSC-derived mature microglia retain their identity and functionally integrate in the chimeric mouse brain. Nat Commun 11:1577.
27. Pepper RE, Pitman KA, Cullen CL, Young KM (2018): How do cells of the oligodendrocyte lineage affect neuronal circuits to influence motor function, memory and mood? Front Cell Neurosci 12:399.
28. Kuhn S, Gritti L, Crooks D, Dombrowski Y (2019): Oligodendrocytes in development, myelin generation and beyond. Cells 8:1424.
29. Boulanger JJ, Messier C (2017): Doublecortin in oligodendrocyte precursor cells in the adult mouse brain. Front Neurosci 11:143.
30. Subramanian A, Tamayo P, Mootha VK, Mukherjee S, Ebert BL, Gillette MA, *et al.* (2005): Gene set enrichment analysis: A

knowledge-based approach for interpreting genome-wide expression profiles. Proc Natl Acad Sci U S A 102:15545–15550.
31. Jeon SJ, Ryu JH, Bahn GH (2017): Altered translational control of fragile X mental retardation protein on myelin proteins in neuropsychiatric disorders. Biomol Ther (Seoul) 25:231–238.
32. Zhao C, Deng W, Gage FH (2008): Mechanisms and functional implications of adult neurogenesis. Cell 132:645–660.
33. Clark PJ, Bhattacharya TK, Miller DS, Rhodes JS (2011): Induction of c-Fos, Zif268, and Arc from acute bouts of voluntary wheel running in new and pre-existing adult mouse hippocampal granule neurons. Neuroscience 184:16–27.
34. Brain A: Atlas: Expression of ARC in the Adult Mouse Brain. Available at: http://mouse.brain-map.org/gene/show/11625. Accesssed November 1, 2022.
35. Brain A: Atlas: Expression of EGR1 in the Adult Mouse Brain. Available at: https://mouse.brain-map.org/gene/show/13431. Accesssed November 1, 2022.
36. Brain A: Atlas: Expression of FOS in the Adult Mouse Brain. Available at: http://mouse.brain-map.org/gene/show/14058. Accesssed November 1, 2022.
37. Rochefort NL, Konnerth A (2012): Dendritic spines: From structure to in vivo function. EMBO Rep 13:699–708.
38. Muller D (2013): Dendritic spines. In: Rubenstein JLR, and Rakic P, editors. Neural Circuit Development and Function in the Brain. Amsterdam: Elsevier.
39. Citri A, Malenka RC (2008): Synaptic plasticity: Multiple forms, functions, and mechanisms. Neuropsychopharmacology 33:18–41.
40. Crane AT, Voth JP, Shen FX, Low WC (2019): Concise review: Human-animal neurological chimeras: Humanized animals or human cells in an animal? Stem Cells 37:444–452.
41. Neuhofer D, Henstridge CM, Dudok B, Sepers M, Lassalle O, Katona I, Manzoni OJ (2015): Functional and structural deficits at accumbens synapses in a mouse model of fragile X. Front Cell Neurosci 9:100.
42. Irwin SA, Patel B, Idupulapati M, Harris JB, Crisostomo RA, Larsen BP, *et al.* (2001): Abnormal dendritic spine characteristics in the temporal and visual cortices of patients with fragile-X syndrome: A quantitative examination. Am J Med Genet 98:161–167.
43. Hodges JL, Yu X, Gilmore A, Bennett H, Tjia M, Perna JF, *et al.* (2017): Astrocytic contributions to synaptic and learning abnormalities in a mouse model of fragile X syndrome. Biol Psychiatry 82:139–149.
44. Linaro D, Vermaercke B, Iwata R, Ramaswamy A, Libé-Philippot B, Boubakar L, *et al.* (2019): Xenotransplanted human cortical neurons reveal species-specific development and functional integration into mouse visual circuits. Neuron 104:972–986.e6.
45. Xu R, Brawner AT, Li S, Liu JJ, Kim H, Xue H, *et al.* (2019): OLIG2 drives abnormal neurodevelopmental phenotypes in human iPSC-based organoid and chimeric mouse models of Down syndrome. Cell Stem Cell 24:908–926.e8.
46. Espuny-Camacho I, Michelsen KA, Gall D, Linaro D, Hasche A, Bonnefont J, *et al.* (2013): Pyramidal neurons derived from human pluripotent stem cells integrate efficiently into mouse brain circuits in vivo. Neuron 77:440–456.